land

Article

Effect of Different Landscapes on Heat Load to Buildings

Ahmed Kanaan [1], Bernd Leinauer [2], Matteo Serena [3], Elena Sevostianova [2], Burl Donaldson [4] and Igor Sevostianov [1,*]

1 Department of Mechanical and Aerospace Engineering, NMSU, Las Cruces, NM 88003, USA; alhrdop@nmsu.edu
2 Department of Plant and Environmental Sciences, NMSU, Las Cruces, NM 88003, USA; leinauer@nmsu.edu (B.L.); esevosti@nmsu.edu (E.S.)
3 Department of Botany and Plant Sciences, University of California Riverside, Riverside, CA 92521, USA; matteos@ucr.edu
4 Energy Analyst, LLC, Albuquerque, NM 87108, USA; abdonalds@gmail.com
* Correspondence: igor@nmsu.edu

Abstract: Strategies to conserve water have been implemented by many municipalities in the US Southwest to minimize quantities of water used for irrigating urban landscapes. Some of them encourage and even enforce homeowners to remove the turfgrass to reduce the irrigation water demands. This strategy not only ignores the numerous benefits derived from the turfgrasses but also fails to recognize the energy savings for the buildings surrounded by green landscapes. Quantitative analysis of the effect and importance of different types of landscapes on urban heat load and the subsequent energy consumption inside those buildings is of great practical need. Field experiments were conducted at New Mexico State University to assess the effect of different landscapes on heat transfer and ambient air and surface temperatures from June 2017 to October 2018. Two standard wood frame walls covered with stucco and surrounded by either Kentucky bluegrass or by hardscape were set up and equipped with sensors, measuring wall and air temperature, relative humidity, wind speed and the solar and far infrared radiation balance. Our results show that overall heat load from the xeric landscape is noticeably higher than the one from the grass landscape. Based on these data, we assessed the potential for energy savings by utilizing turfgrass landscaping.

Keywords: heat island; landscape; heat transfer

check for updates

Citation: Kanaan, A.; Leinauer, B.; Serena, M.; Sevostianova, E.; Donaldson, B.; Sevostianov, I. Effect of Different Landscapes on Heat Load to Buildings. *Land* **2021**, *10*, 733. https://doi.org/10.3390/land10070733

Academic Editor: Nir Krakauer

Received: 1 April 2021
Accepted: 6 July 2021
Published: 13 July 2021
Corrected: 4 February 2022

1. Introduction

In this paper, we quantify the effect of landscaping on the temperature and heat exchange with the external building walls. We compare the combined effects of solar heat, convection and radiation at the walls surrounded by either turfgrass or xeric landscapes. While the amount of direct solar heat is the same for both cases, heat transfer by convection and surface radiation strongly depend on the type of landscape. Namely, this consideration is responsible for the so called "heat island effect". The goal of this study was to evaluate the hypotheses that there is a noticeable difference in total heat flux on the walls of buildings surrounded by turfgrass and xeric landscapes. To the best of our knowledge, there have been no previous quantitative evaluations of the effect of landscape on the heat transfer to urban structures. This quantity is of key importance since it determines the energy consumption for cooling buildings in hot climate zones. We show that grass landscaping can reduce the amount of total heat exchange with urban structures by more than 50% during the daytime in the hot season. These results are especially important in the context of the existing strategies in the US Southwest to minimize quantities of water used for irrigating urban landscapes [1] that do not account for the effects produced by turfgrass on heat loading on buildings [2].

The United States Environmental Protection Agency defines "heat islands" as urban, built-up areas that can be up to 12 °C warmer than adjacent rural areas. Heat islands increase summertime peak energy demand, air conditioning costs, air pollution and greenhouse gas emissions [3]. More critically, the structure and function of urban environmental framework change, influencing the health of urban residents [4,5]. The effect of the heat island is assessed in [6] by using a numerical model. The presence of the urban heat island was first reported over a century ago [7]. Howard's estimations demonstrated the normal urban temperature excess of London to be 2.0 °F, the excess being most prominent around evening time, when it reaches up to 3.7 °F. Moreover, the adjusted surface energy in urban zones essentially alters micro and mesoscale stream fields [8]. In the interim, it is found that China is additionally encountering serious urban heat island effect in many modern cities, particularly as the normal temperature contrast on the outskirt of Beijing was 3.3 °C from 1961 to 2000, and urban heat island impact of Shanghai comes to 7.4 °C [9,10]. By and large, the heat island impact was greatest in the winter and lowest in the spring. During a summer day, the circumstance was reversed with the city being 0.3 °F cooler than the surrounding open country [11]. In San Francisco, the largest heat island effect was estimated, and the temperature contrast between a huge park region and the downtown area was over 10 °C [12,13] demonstrating that the magnitude of the heat island effect is directly connected to the city size. The authors of [14] ascribed the heat island effect essentially to the level of development of the urban environment. Reference [15] underscored the effect of buildings and surface covers as having enormous heat trapping and heat storage capability. The contention is that the city can retain a lot of heat, in contrast to the countryside, during the day, and some of this heat is retained through the night. The data on the heat island effects and the relationship between landscape characteristics and land surface temperature have been summarized in [16]. Further reports show [17,18] that hard surfaces and built structures in urban locations can change neighborhood climate through the urban heat island effect. The impact of these changes could have implications at the regional level [19]. This effect alludes to the generally higher surface temperatures that occur in urban locations due to cover changes and emerging urbanization [20]. The urban heat island effects are for the most part best observed at night, as rates of urban cooling are slower than cooling over a "rural" area due to slower discharge of heat from the developed urban surfaces [21]. Separate to this effect, the total impacts of these changes decrease the change between daytime and nighttime temperatures [22] due to heat capacitance of developed urban areas.

The hotter temperatures likely result in increased air-conditioning use, hence expanding electric power consumption [23]. The expanded urban effect may also debilitate the maintainability of water supplies as in water-stressed locales, urban inhabitants may consume more water for open spaces [24]. Expanded water utilization, moreover, serves as a strategy to moderate high urban temperatures through evapotranspiration [25,26]. Common examination of the urban heat effect is for the most part centered on canopy-layer temperatures, which incorporate the air between the urban surface and offending building height [27]. An exceptional subset examination concentrates on the surface urban heat island, utilizing surface temperature, deduced size [28–30] and its relation to urban surface physical characteristics [31].

The urban cover, or spatial composition within the city locations (i.e., the relative sums of the component cover, such as timberland compared to concrete surfaces [32]), is critical in deciding the intra-urban effect [33,34]. The field of local environment effect has long been concerned with measuring spatial arrangement and has measured the spatial characteristics of cover patches and their connections to one another [35,36]. Minimization of urban heat island and the rate of surface zone secured by green vegetation is discussed in [37]. Urban temperature, particularly surface temperature, is a vital aspect of urban surface and one of the foremost variables influencing urban climate, regulating and controlling different environmental forms [38,39]. Urban locations involve a significantly diverse climatology compared to their rural locations [40,41]. The physical properties of cities and buildings result in altered surface radiation and heating budget, which needs to be accounted for in modeling considerations [42,43]. To begin with, building clusters influence solar radiation such that different reflections between buildings and streets affect radiation to space. In this manner, cities ordinarily have a lower albedo than crops or grasses. It is obvious that the perspective proportion of building stature to street width may be a parameter for the sky view [44–46]. We investigated the effect of different landscapes (irrigated turf vs. non-irrigated xeric or hardscape) on ambient air temperature and heat flux of building surrounds in the desert Southwest. From these temperature data we can model several scenarios of the energy requirements to cool or heat the buildings. Despite these documented heat-island effects, no research has been performed to determine the consequences in terms of overall energy consumption associated with these strategies. Research is needed to quantify the effect and importance of different types of landscapes on urban ambient temperatures around buildings and the subsequent energy consumption inside those buildings.

2. Materials and Methods

2.1. Materials

A study was conducted at New Mexico State University (NMSU) (USDA Plant Hardiness Zone 8) from June 2017 to October 2018 to investigate the effect of irrigated turf and non-irrigated xeric landscapes on heat transfer and air and surface temperatures of residential walls. Monthly average air temperatures, precipitation and reference evapotranspiration for short grass (ETos) during the research period were collected at a weather station located in close proximity to the study site, and these are listed in Tables 1 and 2.

Table 1. Monthly climate data and reference evapotranspiration for short grass (ETos) at the research site during 2017.

Month	Temp Max		Temp Min		Temp Avg.		Precipitation		ET_{OS}	
	C	F	C	F	C	F	mm	in	mm	in
June	36.6	98	20.0	68	28.3	83	1.3	0.1	242	9.5
July	34.3	94	21.2	70	27.8	82	82.3	3.2	213	8.4
August	32.8	91	19.7	68	26.3	79	45.0	1.8	186	7.3
September	31.8	89	17.3	63	24.5	76	6.9	0.3	158	6.2
October	27.2	81	11.9	53	19.5	67	24.4	1.0	130	5.1
November	23.4	74	6.8	44	15.1	59	8.4	0.3	78	3.0
December	16.2	61	0.1	32	8.2	47	2.3	0.1	51	2
Total							171	6.8	1058	41.5

Table 2. Monthly climate data and reference evapotranspiration for short grass (ETos) at the research site during 2018.

Month	Temp Max		Temp Min		Temp Avg.		Precipitation		ET_{OS}	
	C	F	C	F	C	F	mm	in	mm	in
January	16.0	61	−1.0	30	7.5	45	0.3	0.01	67	2.7
February	19.1	66	3.6	38	11.3	52	15.8	0.62	84	3.3
March	22.6	73	6.3	43	14.5	58	1.5	0.06	138	5.4
April	27.8	82	11.4	53	19.6	67	0.0	0.00	198	7.8
May	33.1	92	14.9	59	24.0	75	0.0	0.00	228	9.0
June	36.9	98	20.7	69	28.8	84	14.7	0.58	241	9.5
July	35.3	95	21.4	71	28.3	83	46.7	1.84	200	7.9
August	34.6	94	21.2	70	27.9	82	26.9	1.06	183	7.2
September	24.6	76	31.3	88	17.8	64	36.8	1.45	129	5.1
October	23.2	74	11.8	53	17.5	64	57.67	2.27	87	3.4
Total							200	7.9	1555	61.3

Two identical wood frame walls measuring 2.0 × 2.0 m and covered with stucco were set up on two different landscape surfaces. The walls were covered with stucco approximately 0.125 m thick. They were built following standards for the area (14.7.4

NMAC, 2009 New Mexico Earthen Building Materials Code; filed 28 December 2010, repealed 15 November 2016). Both walls were located at the same elevation facing south and were surrounded by either grass or gravel (xeriscape) with no other structures to avoid possible border effects. The first wall was placed on Kentucky bluegrass (*Poa pratensis* L.), located at New Mexico State University's turfgrass research facility (Figure 1a). The second frame was positioned on light gravel mixed with coarse crushed rocks with no vegetation. The area was part of a xeric landscape on NMSU's campus, located about 500 m northwest from the turfgrass research facility (Figure 1b).

(a) (b)

Figure 1. Stucco covered wooden framed wall surrounded by turfgrass (**a**) and hardscape (**b**).

Kentucky bluegrass (20 by 30 m) was irrigated during the growing season by means of Toro pop-up sprinkler heads at 100% of reference evaporation for short grass (ETos). During winter months, the area was irrigated once every two weeks. Kentucky bluegrass was mowed two to three times per week at a height of 7.5 cm with clippings collected, and the grass was fertilized at recommended application rates to prevent nutrient stress. Sensors measuring wall and air temperatures, relative humidity, wind speed and the solar and far infrared radiation balance were placed to take relevant measurements. The sensors were connected to data loggers housed in weatherproof enclosures and located near the structures. All data were recorded every 30 min and averaged over one hour by means of a CR1000 logger (Campbell Scientific Inc., Logan, UT, USA). The battery of the logger was recharged using a solar panel. Manufacturers and accuracy of measurements are summarized in Table 3.

Table 3. Sensors used in the study to measure wall and air temperature, humidity, wind and radiation at the turf site (Location 1) and xeric landscape site (Location 2).

	Measured Parameter	Sensor Type	Accuracy	Brand, Model and Manufacturer Location
(a)	Wall temperature	Thermocouples	±0.5%	Type E, REOTEMP Instruments Corp., San Diego, CA, USA
(b)	Reference air temperature	Rugged temperature probe	±0.2 °C	107, Campbell Scientific Inc., Logan, UT, USA
(c)	Air temperature	Pendant temperature Data logger	±0.53 °C	Hobo, UA-002, Bourne, MA, USA
(d)	Relative humidity	Temperature and relative humidity probe	±2%	CS215, Campbell Scientific Inc., Logan, UT, USA
(e)	Wind speed and direction	Three-cup anemometer	Range of 0 to 45 m/s (0 to 100 mph).	014A, Campbell Scientific Inc., Logan, UT, USA
(f)	Solar and far infrared radiation balance	Blackened thermopile	Spectral range: 0.2 to 100 µm Directional error (0 to 60 °C at 1000 W·m^{-2}): <30 W·m^{-2}	NR-LITE2, Campbell Scientific Inc., Logan, UT, USA

(a) Wall temperature was continually recorded by four thermocouples equipped with radiation shields and mounted to each wall: two thermocouples were placed 0.8 m apart at a height of 0.5 m and two placed 0.8 m apart at a height of 1.00 m above ground.
(b) Temperature and the reference temperature were incorporated into the measurement (CR1000 Data logger operator's manual, Campbell Scientific Inc., Logan, UT, USA). The reference air temperature sensor 107 temperature probe (BetaTherm 100K6A1IA Thermistor) was installed and housed in a radiation shield on the wall on the north-facing side (shade measurement) at a height of 2 m.
(c) To measure air temperature above the landscape, two Hobo pendant loggers (Temperature/Light Data Logger) with shields were used at the distance of 10 m from the wall at heights of 0.5 and 1.0 m. The logger uses a coupler and optical base station with USB interface for launching and data readout with a computer.
(d) Relative humidity sensors were installed and covered with shields on top of both walls at a height of 2.0 m.
(e) Wind speed and direction were measured at a height of 2.0 m using a 014A three-cup anemometer at the turfgrass facility weather station. The anemometer monitored horizontal wind speed for the range of 0 to 45 m s^{-1} with a threshold of 0.45 m s^{-1} and was connected directly to a Campbell Scientific datalogger, which measured the 014A's pulse signal and converted it to mph or m s^{-1}.
(f) A NR-LITE2 thermopile sensor was used for measuring solar and infrared radiation net radiation exchange (i.e., both short wave and long-wave components). The NR-LITE2 was installed on the south-facing side of the walls at a height of 2.0 m.

2.2. Methods

In steady operation, heat transfer between the landscapes to the walls by convection, net environmental radiation and solar radiation is equal to the heat transfer into the wall and ultimately into the house or building. Data are used to calculate heat transfer rate Q ($W \cdot m^{-2}$) on the outside of the walls, which is a contributing factor to temperature changes inside buildings. Unit area heat transfer rate or thermal flux, also referred to as heat flow rate intensity, is a rate of energy flow per unit of area.

The total heat exchange with the walls consists of three components, illustrated in Figure 2 and expressed in Equation (1).

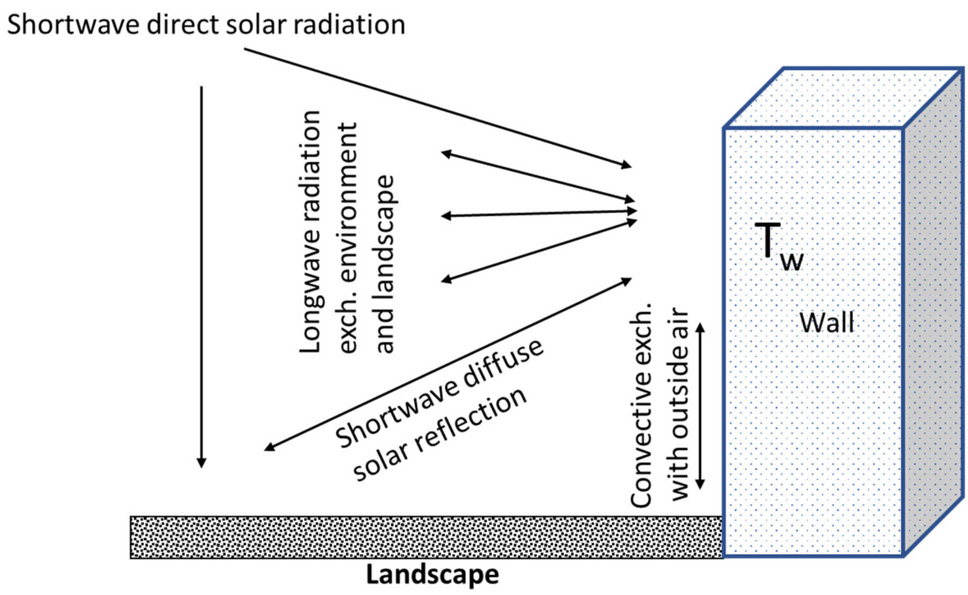

Figure 2. The heat balance on the outside the wall.

$$\mathrm{Q} = \mathrm{Qconv.} + \mathrm{Qrad.} + \mathrm{Qsolar} \tag{1}$$

Qconvection is the flow of heat through bulk, macroscopic movement of fluid from a hot region to a cool region, as opposed to the microscopic transfer of heat between atoms involved as in conduction. The free convection with air surrounding the wall can be expressed as

$$\mathrm{Qconvection} \; = \mathrm{h}\;(\mathrm{Tas} - \mathrm{Tw}) \tag{2}$$

where (h) is the convective heat transfer coefficient of the process ($\mathrm{W{\cdot}m^{-2}\,{}^{\circ}C^{-1}}$), and (Tw) and (Tas) are the average temperatures of the four thermocouples mounted on the wall and the surrounding air temperature, respectively. An experiment was conducted at New Mexico State University (USDA Plant Hardiness Zone 8); a nominal free convection coefficient of 5 $\mathrm{W/m^2}$-C is assumed for both walls. Surface radiation, Qradiation, is propagated by electromagnetic waves mainly in the infrared region. Radiation emitted by a body is a consequence of thermal agitation of its composing molecules and can be generally expressed by:

$$\mathrm{Qradiation} \; = \epsilon' \sigma \left(\mathrm{Tas}^4 - \mathrm{Tw}^4\right) \tag{3}$$

It must be noted that the temperatures appearing in Equation (3) must be in absolute units (kelvin). The emissivity coefficient (ϵ) of the turfgrass and hardscape is uniquely related to the surfaces and for radiation exchange between two grey surfaces:

$$\epsilon' = \frac{1}{\left(\frac{1}{\varepsilon\ \mathrm{wall}}\right) + \left(\frac{1}{\epsilon\ \mathrm{landscape}}\right) - 1} \tag{4}$$

The Stefan–Boltzmann constant in imperial units is σ = 5.6703·10^{-8} ($\mathrm{W{\cdot}m^{-2}K^{-4}}$). We also used the emissivity coefficient, ϵ = 0.9 for the grass and 0.95 for the xeric landscape [47]. Note that radiation exchange is between surfaces, so it is assumed that surrounding surfaces seen by the wall are the same as air temperature (we recognize this as an approximation). Equations (3) and (4) can be used to calculate radiation in either direction, depending on which surface temperature is highest. In a rigorous treatment, radiation is very complex, in that exchange is with surfaces at different temperatures and with different view factors. Hence, for tractable calculations, simplifications were made. Qsolar irradiance is the power per unit area received from the sun in the form of electromagnetic radiation in the wavelength range of the measuring instrument. The solar irradiance integrated over time is called solar irradiation or solar exposure, expressed as:

$$\mathrm{Qsolar} = (1 - \alpha) * \mathrm{view\ factor} * \mathrm{qr} \tag{5}$$

The absorptivity α is an optical property of a landscape, which describes how much radiation was absorbed in relation to amount of radiant energy incident on the surface. The values used for the absorptivity of the grass and xeric landscaping are 0.7 and 0.38, respectively. Radiation absorption occurs for optically opaque materials on their surface and for semi-transparent materials on the surface and in the bulk of the material. For the landscape, radiation transmission is zero, so the radiant energy, which is not absorbed, is reflected, or $(1 - \alpha)$. The walls surrounding both landscapes are assumed to see 50% of the landscape below the horizon and 50% above the horizon, so a view factor of 0.5 was applied for coupling the landscape radiant exchange with the walls. Since the horizon for both landscapes is the same, the component of radiation above the horizon was not included in the current analysis for simplicity. Appendix A contains all the data from June 2017 to October 2018 as shows in Figures A1–A4 (average temperatures for wall and surrounding air, net radiation, wind speed and relative humidity) for both grass and xeric landscapes. In addition, we used the weather station at New Mexico State University's turfgrass research center, which measured the actual real time solar flux which arrives at the ground surface, for values of qr.

3. Results

3.1. The Overall Heat Fluxes

We applied Equations (1)–(4) to calculate the rate of heat exchange with the walls according to the directions shown in Figure 2 and followed the numerical modeling presented in detail by [47]. After that we calculated the average of the rate of energy received by the wall for each month of study during daytime (8:00 a.m.–8:00 p.m.) and nighttime (8:30 p.m.–7:30 a.m.) and these results are shown in Figure 3. Figure 3 illustrates average heat transfer received by the two walls under study: one surrounded by a xeric landscape and one surrounded by a grass landscape in the period from June 2017 to October 2018. The solar irradiation produces the main effect on the amount of the heat flux; we evaluated the heat flux at two different times from (8:00 a.m.–8:00 p.m.) and (8:30 p.m.–7:30 a.m.). The highest heat flux in 2017 was in June and August and in 2018 in May and June; the lowest heat flux was in October 2017 and 2018. Figure 3 illustrates comparison of the heat flux at two landscapes. Note that direct solar does not account for the calculation since both walls experience the same exposure. In contrast, diffuse reflected solar radiation was included since the two landscapes have differing radiative characteristics. The walls are assumed to exchange longwave radiation with the environment, but the environment is divided into two regions: the hemisphere below the horizon and the hemisphere above the horizon. Since the hemisphere above the horizon is the same for both walls, that component was not included in the calculation. The hemispheres below the horizon are different for two walls because of the different radiation properties between the two landscapes, and a view factor of 0.5 was used, based on the assumption that the landscape area immediately in front of the wall represents the major portion of the lower hemisphere that the wall "sees". The value for solar radiation that is used in the calculation is based on actual hourly and daily measurements at the latitude corresponding to the experiment. Other calculations are based on recorded data but averaged over daytime and nighttime separately. These daily values were folded into an average heat flux for the period shown in the figure, ~1 month. Another approximation is the assumption that the landscape temperature for longwave radiation exchange is the same as the air temperature above the ground plane. Thus, since some heat exchange components are included in the calculations, values shown in Figure 3 are not as absolute values and serve for comparison only.

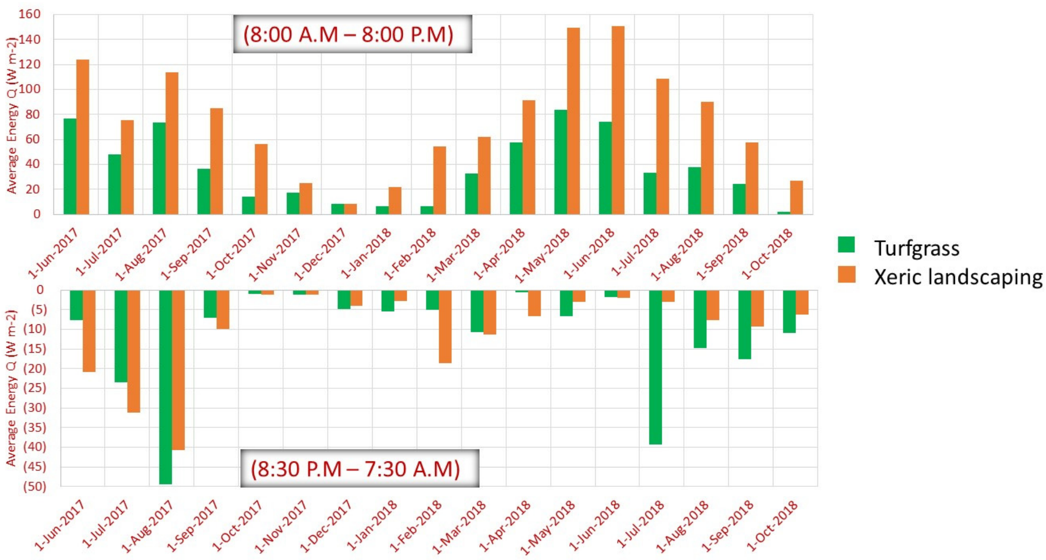

Figure 3. Monthly heat transfer Q from different landscapes during 2017 and 2018 (daytime top and nighttime bottom) from June 2017 to October 2018.

3.2. Heat Transfer to Walls and Solar Radiation Effect

To determine the effect of the solar radiation on the amount of heat transferred to the wall we chose one hot and one cold month (2017 and 2018) using data shown in Figure 3. Both walls were at the same angle as the solar receiver, where the walls were placed in a way that allowed them to receive most of the solar radiation throughout the day, i.e., maximum irradiation at solar noon. After that, we used the weather station at New Mexico State University to obtain the solar radiation in these months, as shown in Figure 4. Taking June 21 and October 5 as representative hot and cold days in 2017 and 2018, we note the difference on June 21 between grass and xeric landscapes to be ~25 W·m^{-2} in 2017 and ~110 W·m^{-2} in 2018 in the peak time (10:00 a.m.–4:00 p.m.) with solar radiation ~1000 W·m^{-2} in both 2017 and 2018. For October 5 in both 2017 and 2018 the difference between landscapes was ~15 and the average solar radiation was ~750 W·m^{-2}.

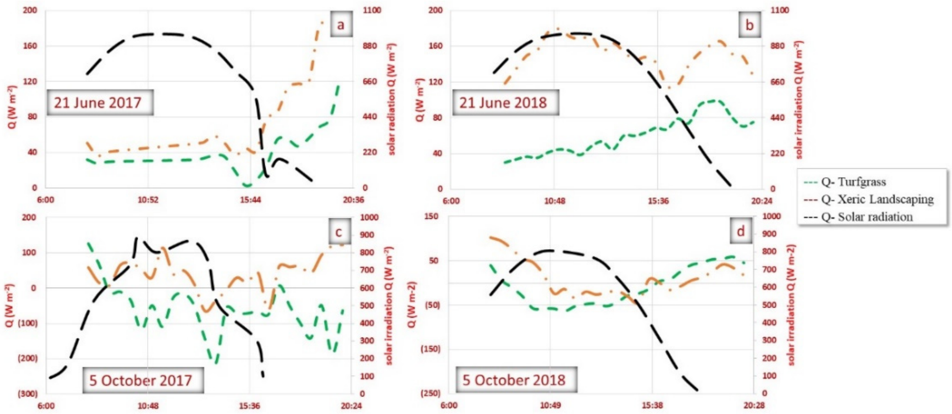

Figure 4. Heat transfer and solar radiation from different landscapes on June 21, 2017 and 2018 (**a**,**b**); and on October 5 (**c**,**d**) in 2017 and 2019.

3.3. Wall Temperature and Relative Humidity

The relative humidity is the ratio of the current absolute humidity to the highest possible absolute humidity, which depends on the current air temperature. The effect of relative humidity on wall temperatures can be examined independently. The change in relative humidity can affect the thermocouple (E type) located on the wall. Figure 5 illustrates the relationship between measured relative humidity and the mean wall temperature. One can see that there is no certain correlation pattern between the curves. For 21 June 2017 we see positive correlation while other three plots indicate negative correlation. The effect could be better illustrated by plotting the difference in mean wall temperature of the two landscapes vs. relative humidity.

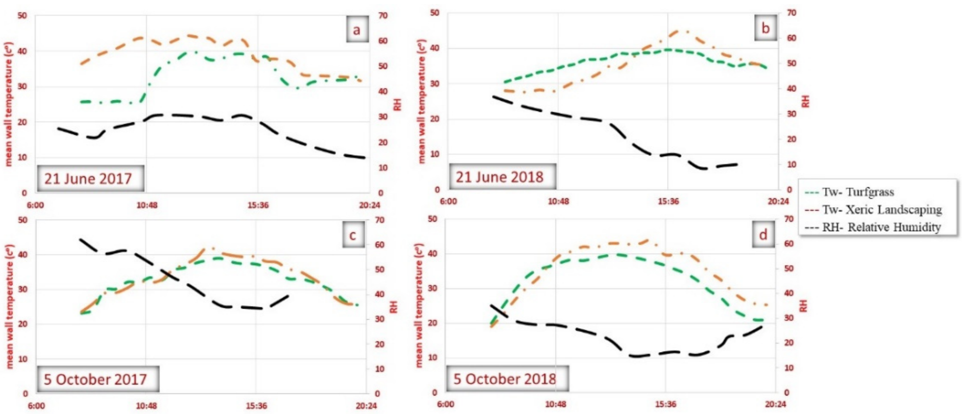

Figure 5. Mean wall temperature (Tw) and relative humidity on walls surrounded by different landscapes (**a**,**b**) in June and (**c**,**d**) in October 2017 and 2018.

3.4. Air Temperature Surrounded and Wind Speed

Convective heat exchange to the walls, according to Equation (2), depends on the convective heat transfer coefficient and the wind speed because h is influenced by wind speed in addition to buoyant flow of air rising from the hot ground. In this case, we need to study the effect of wind speed and the surrounding landscape air temperature. Figure 6 illustrates this relationship between wind speed and surrounded air temperature, Tas. While it would be reasonable to expect that higher wind speed should narrow the wall temperature difference, this conjecture cannot be supported by the data in Figure 6.

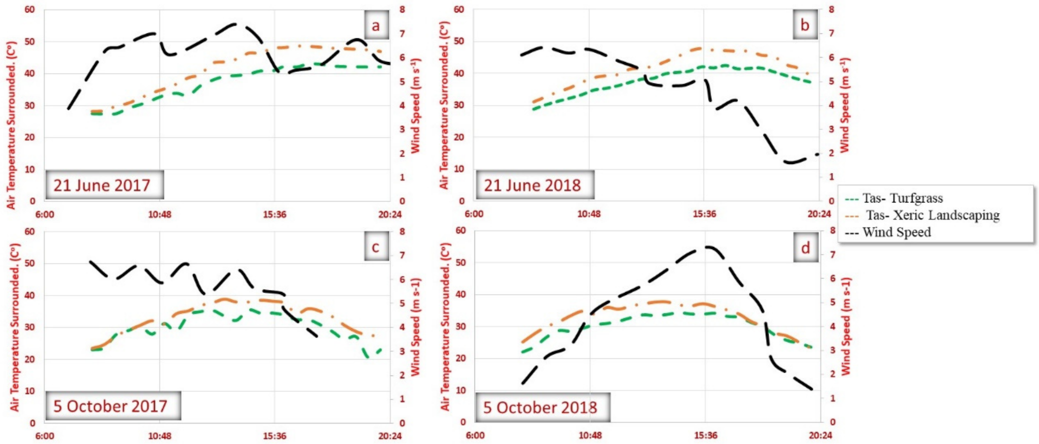

Figure 6. Surrounding air temperature (Tas) and wind speed from different landscapes (**a**,**b**) in June and (**c**,**d**) in October 2017 and 2018.

4. Discussion

The experimental results show that cumulative average heat fluxes acting on the wall surrounded by the xeric landscape are 124 and 113 W·m^{-2} in June and August of 2017 and 149 and 151 W·m^{-2} in May and June of 2018. For the grass landscape in the same periods of time, the monthly average heat fluxes are substantially lower: 76 and 73 W·m^{-2} in June and August of 2017 and 83 and 73 W·m^{-2} in May and June of 2018. The difference between the grass and xeric landscape in June 2017 and 2018 is ~64 W·m^{-2}. This means that urban areas are affected by this increase and cause an increase in the urban temperature. The building surrounded by the xeric landscape is also affected by the amount of heat transferred, which leads to an increase in the heat load inside the building. The lowest heat transfer month in both 2017 and 2018 years was October, as shown in Figure 3. The cumulative heat fluxes acting on the wall surrounded by the xeric landscape in Octobers of 2017 and 2018 were 56 and 26 W·m^{-2}, respectively. The cumulative heat fluxes acting on the wall surrounded by the grass landscape during the same months were 14 W·m^{-2} in 2017 and 2 W·m^{-2} in 2018. These results are influenced by the heat capacities of the two landscapes and their retained heat. In other words, the xeric landscape stores heat during the hot daytime and radiates during nighttime. The xeric landscape has the highest heat exchange with the walls because of its elevated temperature and radiative properties. In this case, the xeric landscape adds between 150 to 100 W·m^{-2} in the hot season and 50 to 20 W·m^{-2} in the cold season to the building surrounded by the xeric landscape. This indicates that walls surrounded by the xeric landscape increase the temperatures in urban areas, and this causes the urban heat island impact [47]. This effect is also called the difference of land surface temperature (LST) in urban relativity [48].

5. Conclusions

The results presented in this study clearly show the effect of landscape on heat effects on a wall under a variety of real environmental conditions. While it is not possible to modify the landscape in built-up metropolitan areas, in single family dwellings, the landscape is generally under the control of the landowner, unless covenants or city ordinances prevent such choices. In consideration of the total effect of landscape choices, however, it would appear that xeriscaping is not necessarily the choice that minimizes both energy and water consumption. This argument is particularly germane in semi-arid areas where municipalities have encouraged conversion of lawns to xeriscape, solely based on water consumption devoted to lawns, shrubbery and trees. It is beyond argument that trees can have a very beneficial effect in shading of walls and roofs when the foliage has developed. Hence, there can be a discussion of the pros and cons of conversion to xeriscape based on the information presented in this study.

Author Contributions: A.K.: Investigation, writing—original draft; E.S.: Methodology, Writing original draft; B.D.; formal analysis, validation, writing—review and editing, I.S.: Conceptualization, supervision, writing—review and editing; B.L.: Conceptualization, funding, supervision; M.S.: data collection, infrastructure, research site. All authors have read and agreed to the published version of the manuscript.

Funding: E.S. acknowledges Support of NASA through CAN 80NSSC20M0034 to NMSU; I.S. acknowledges support of NASA through CAN NNX15AL51H to NMSU. Lawn Institute and National Science Foundation's Engineering Research Center for Re-inventing the Nation's Urban Water Infrastructure, ReNUWIt, Project # 128027 (ID 26975) and NSF EEC-1028968 to Ahmed Kanaan and Elena Sevostianova, respectively.

Institutional Review Board Statement: Not applicable.

Informed Consent Statement: Not applicable.

Data Availability Statement: Data available on request due to restrictions, e.g., privacy and ethical.

Acknowledgments: Support for this study was provided by New Mexico State University's Facilities and Services and by New Mexico State University's Agricultural Experiment Station. The authors are further grateful for the donations from Helena Chemical Company. Review and technical input were provided by Sandia National Laboratories, in particular Walter Gill, who is well versed in radiation heat transfer.

Conflicts of Interest: The authors declare no conflict of interest.

Appendix A

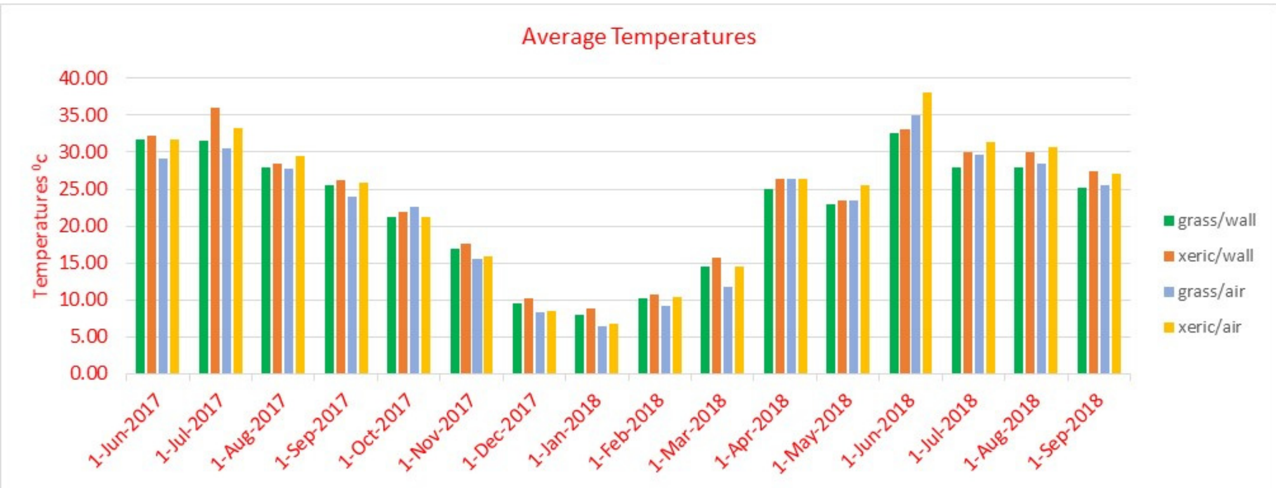

Figure A1. Monthly average temperature for wall and air surrounded by different landscapes (grass and xeric) June 2017 to October 2018.

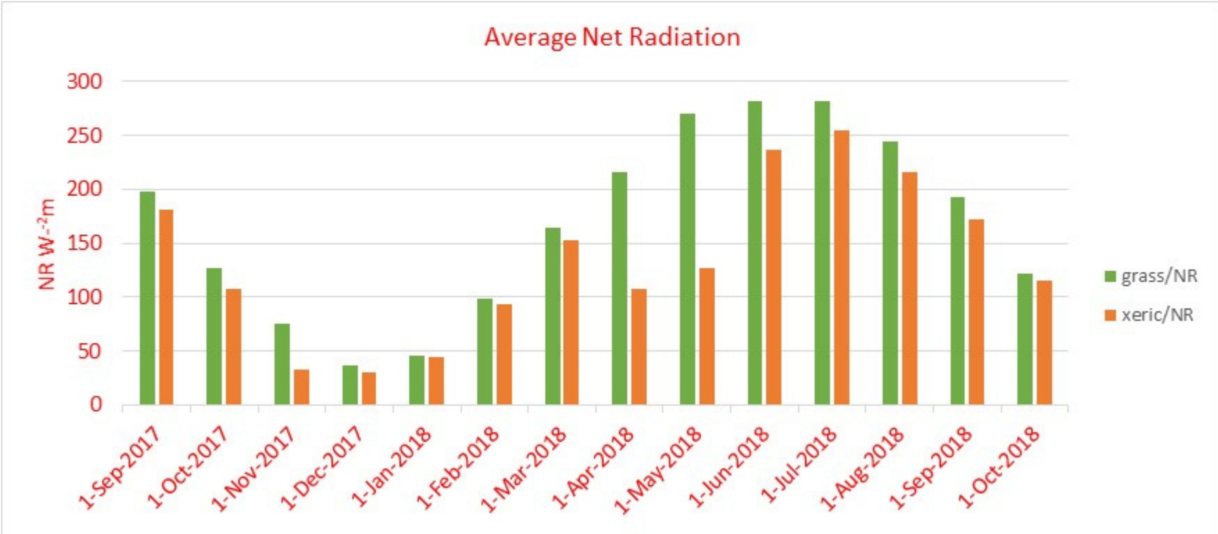

Figure A2. Monthly average net radiation for different landscapes (grass and xeric) September 2017 to October 2018.

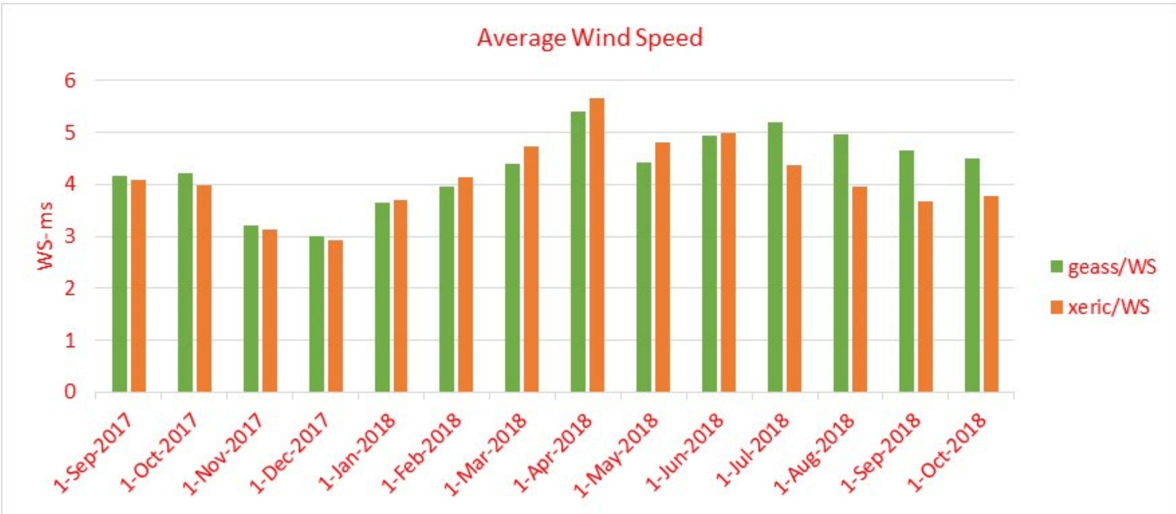

Figure A3. Monthly average wind speed for different landscapes (grass and xeric) September 2017 to October 2018.

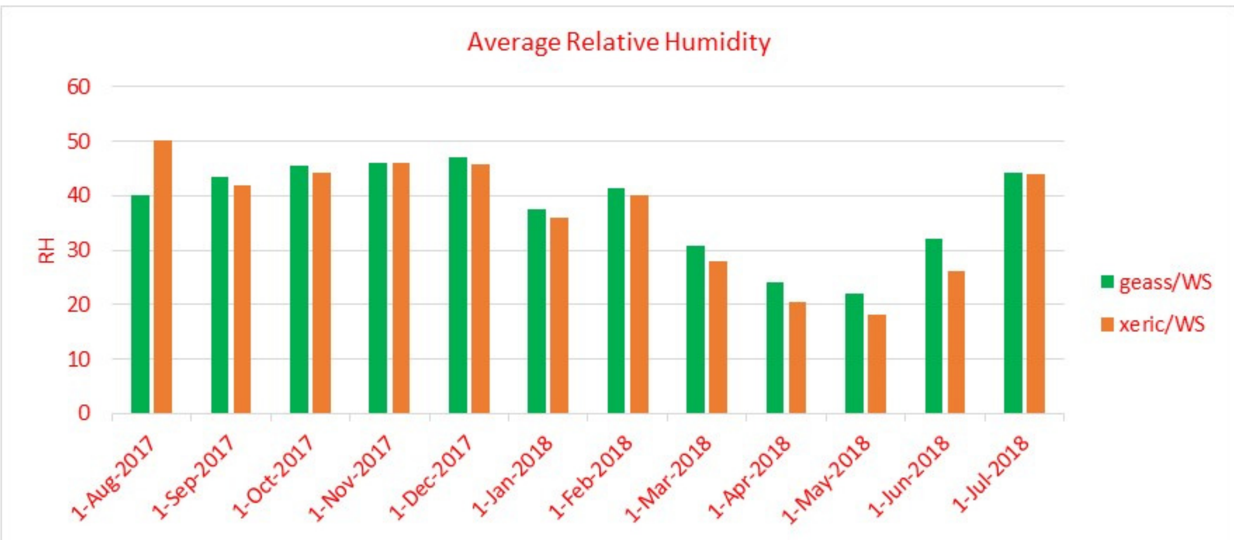

Figure A4. Monthly average relative humidity for different landscapes (grass and xeric) August 2017 to July 2018.

References

1. Devitt, D.A.; Carstensen, K.; Morris, R.L. Residential Water Savings Associated with Satellite-Based ET Irrigation Controllers. *J. Irrig. Drain. Eng.* **2008**, *134*, 74–82. [CrossRef]
2. Beard, J.B.; Green, R.L. The Role of Turfgrasses in Environmental Protection and Their Benefits to Humans. *J. Environ. Qual.* **1994**, *23*, 452. [CrossRef]
3. Bijoor, N.S.; Czimczik, C.I.; Pataki, D.E.; Billings, S.A. Effects of temperature and fertilization on nitrogen cycling and community composition of an urban lawn. *Glob. Chang. Biol.* **2008**, *14*, 2119–2131. [CrossRef]
4. Fu, X.P.; Mou, B.; Griffy-Brown, C. The combination of digital technology and architectural design to develop a process for enhancing energy-saving: The case Maanshan China. *Technol. Soc.* **2014**, *39*, 77–87.
5. Zhao, D.X.; Johnson, C.; Mou, B. Social problems of green buildings: From the humanistic needs to social acceptance. *Renew. Sustain. Energy Rev.* **2015**, *51*, 1594–1609. [CrossRef]
6. Myrup, L.O. A Numerical Model of the Urban Heat Island. *J. Appl. Meteorol.* **1969**, *8*, 908–918. [CrossRef]
7. Howard, L. The Climate of London Deduced from Meteorological Observations Madw. In *Metropolis and at Various Places Around*, 2nd ed.; London, J., Arch, A., Eds.; Harvey and Darton, J. and A. Arch, Longman, Hatchard, S. Highley [and] R. Hunter: London, UK, 1833.
8. Bornstein, R. Mean diurnal circulation and thermodynamic evolution of urban boundary layers. *Model. Urban Bound. Layer Amer. Meteor. Soc.* **1987**, *7*, 53–94.
9. Tran, H.; Uchihama, D.; Ochi, S.; Yasuoka, Y. Assessment with satellite data of the urban heat island effects in Asian mega cities. *Int. J. Appl. Earth Obs. Geoinf.* **2006**, *8*, 34–48. [CrossRef]
10. Yang, L.; He, B.J.; Ye, M. Application research of ECOTECT in residential estate planning. *Energy Build.* **2014**, *72*, 195–202. [CrossRef]
11. Chandler, T.J. London's urban climate. *Geography. J.* **1962**, *127*, 279–302. [CrossRef]
12. Duckworth, F.S.; Sandberg, J.S. The Effect of Cities upon Horizontal and Vertical Temperature Gradients. *Bull. Am. Meteorol. Soc.* **1954**, *35*, 198–207. [CrossRef]
13. Landsberg, H.E. The Climate of Towns. In *Man's Role in Changing the Face of the Earth*; Thomas, W.L., Jr., Ed.; University of Chicago Press: Chicago, IL, USA, 1956; p. 1193.
14. Kratzer, P.A. *Das Stadtklima Die Wissenshaft, Braunschweig, Friedr*; Vieweg Sohn: Heidelberg, Germany, 1956; Volume 90, p. 184.
15. Michell, J.M. The temperature of cities. *Weatherwise* **1961**, *14*, 224–229. [CrossRef]
16. Connors, J.P.; Galletti, C.S.; Chow, W.T.L. Landscape configuration and urban heat island effects: Assessing the relationship between landscape characteristics and land surface temperature in Phoenix, Arizona. *Landsc. Ecol.* **2012**, *28*, 271–283. [CrossRef]
17. Oke, T.R. *Boundary Layer Climates*, 2nd ed.; Routlede: London, UK, 1987.
18. Quattrochi, D.A.; Ridd, M.K. Measurements and analysis of thermal energy responses from discrete urban surfaces using remote sensing data. *Int. J. Remote. Sens.* **1994**, *15*, 1991–2002. [CrossRef]
19. Kalnay, E.; Cai, M. Impact of urbanization and land-use on climate. *Nature* **2003**, *423*, 528–531. [CrossRef] [PubMed]
20. Oke, T.R. The Heat Island of the Urban Boundary Layer: Characteristics, Causes and Effects. In *Wind Climate in Cities*; Cermak, J.E., Ed.; Kluwer Academic Publishers: Dordrecht, The Netherlands, 1995.
21. Quattrochi, D.; Luvall, J.; Rickman, D.; Estes, M.; Laymon, C.; Howell, B. A decision support information system for urban landscape management using thermal infrared data. *Photogram Eng.* **2000**, *66*, 1195–1207.
22. Landsberg, H.E. *The Urban Climate*; National Academy Press: New York, NY, USA, 1981.
23. Gober, P.; Wentz, E.A.; Lant, T.; Tschudi, M.K.; Kirkwood, C.W. WaterSim: A simulation model for urban water planning in Phoenix, Arizona, USA. *Environ. Plan.* **2011**, *38*, 197–215. [CrossRef]
24. Goward, S.N.; Cruickshanks, G.D.; Hope, A.S. Observed relation between thermal emission and reflected spectral radiance of a complex vegetated landscape. *Remote. Sens. Env.* **1985**, *18*, 137–146. [CrossRef]
25. Gober, P. *Metropolitan Phoenix: Place Making and Community Building in the Desert*; University of Pennsylvania: Philadelphia, PA, USA, 2006.
26. Oke, T.R. *Initial Guidance to Obtain Representative Meteorological Observations at Urban Sites*; IOM Report 81.TD; World Meteorological Organization: Geneva, Switzerland, 2004.
27. Nichol, J.E. Fine resolution surface temperature patterns related to urban morphology in a tropical city: A satellite-based study. *J. Appl. Meteorol.* **1996**, *35*, 135–152. [CrossRef]
28. Zhang, X.; Zhong, T.; Feng, X.; Wang, K. Estimation of the relationship between vegetation patches and urban land surface temperature with remote sensing. *Int. J. Remote. Sens.* **2009**, *30*, 2105–2118. [CrossRef]
29. Jin, M.S. Developing an index to measure urban heat island effect using satellite land skin temperature and land cover observation. *J. Clim.* **2012**, *25*, 6193–6201. [CrossRef]
30. Voogt, J.A.; Oke, T.R. Thermal remote sensing of urban climates. *Remote. Sens. Environ.* **2003**, *86*, 370–384. [CrossRef]
31. Gustafson, E.J. Quantifying landscape spatial pattern: What is the state of the art. *Ecosystems* **1998**, *1*, 143–156. [CrossRef]
32. Rosenzweig, C.; Solecki, W.; Parshall, L.; Chopping, M.; Pope, G.; Goldberg, R. Characterizing the urban heat island in current and future climates in New Jersey. *Glob. Env. Chang.* **2005**, *6*, 51–62. [CrossRef]
33. Steeneveld, G.J.; Koopmans, S.; Heusinkveld, B.G.; van Hove, L.W.A.; Holtslag, A.A.M. Quantifying urban heat island effects and human comfort for cities of variable size and urban morphology in the Netherlands. *J. Geophys. Res.* **2011**, *116*. [CrossRef]

34. Blocken, B.; Stathopoulos, T.; Carmeliet, J. CFD simulation of the atmospheric boundary layer: Wall function problems. *Atmos. Environ.* **2007**, *41*, 238–252. [CrossRef]
35. Li, F.; Wang, R.; Paulussen, J.; Liu, X. Comprehensive concept planning of urban greening based on ecological principles: A case study in Beijing, China. *Landsc. Urban Plan.* **2005**, *72*, 325–336. [CrossRef]
36. Zhou, W.; Huang, G.; Cadenasso, M.L. Does spatial configuration matter? Understanding the effects of land cover pattern on land surface temperature in urban landscapes. *Landsc. Urban Plan.* **2011**, *102*, 54–63. [CrossRef]
37. McGarigal, K.; Marks, B.J. *FRAGSTATS: Spatial Pattern Analysis Program for Quantifying Landscape Structure*; General Technical Report PNW-GTR-351; Pacific Northwest Research Station, USDA-Forest Service: Portland, OR, USA, 1995.
38. Turner, M.G.; Gardner, R.H.; O'Neill, R.V. *Landscape Ecology in Theory and Practice*; Springer: New York, NY, USA, 2001.
39. Oke, T.R. The energetic basis of the urban heat island. *Q. J. R. Meteorol. Soc.* **1982**, *108*, 1–24. [CrossRef]
40. Godowitch, J.M.; Ching, J.K.S.; Clarke, J.F. Evolution of the nocturnal inversion layer at an urban and nonurban site. *J. Clim. Appl. Meteorol.* **1985**, *24*, 791–804. [CrossRef]
41. Grimmond, C.S.B. The International Urban Energy Balance Models Comparison Project: First results from phase 1. *J. Appl. Meteorol. Climatol.* **2010**, *49*, 1268–1292. [CrossRef]
42. Grimmond, C.S.B. Initial results from phase 2 of the international urban energy balance comparison project. *Int. J. Climatol.* **2011**, *31*, 244–272. [CrossRef]
43. Svensson, M.K. Sky view factor analysis-implications for urban air temperature differences. *Meteorol. Appl.* **2004**, *11*, 201–211. [CrossRef]
44. Ali-Toudert, F.A.; Mayer, H. Numerical study on the effects of aspect ratio and orientation of an urban street canyon on outdoor thermal comfort in hot and dry climate. *Build. Env.* **2006**, *41*, 94–108. [CrossRef]
45. Kanda, M. Progress in urban meteorology. *J. Meterol. Soc. Jpn.* **2007**, *85*, 363–383. [CrossRef]
46. Yaghoobian, N.; Kleissl, J.; Krayenhoff, E.S. Modeling the Thermal Effects of Artificial Turf on the Urban Environment. *J. Appl. Meteorol. Climatol.* **2010**, *49*, 332–345. [CrossRef]
47. Renard, F.; Alonso, L.; Fitts, Y.; Hadjiosif, A.; Comby, J. Evaluation of the Effect of Urban Redevelopment on Surface Urban Heat Islands. *Remote. Sens.* **2019**, *11*, 299. [CrossRef]
48. Zhou, D.; Xiao, J.; Bonafoni, S.; Berger, C.; Deilami, K.; Zhou, Y.; Sobrino, J. Satellite Remote Sensing of Surface Urban Heat Islands: Progress, Challenges, and Perspectives. *Remote. Sens.* **2018**, *11*, 48. [CrossRef]